Deliverable D 2.4
Mechanical data for the finite element simulation

Document type	**Deliverable D 2.4**
Document Version / Status	**5.2**
Primary Authors	**Dietmar Gruber, dietmar.gruber@unileoben.ac.at, MUL**
Distribution Level	**PU (Public)**
Project Acronym	**ATHOR**
Project Title	**Advanced THermomechanical multiscale mOdelling of Refractory linings**
Grant Agreement Number	**764987**
Project Website	**www.etn-athor.eu**
Project Coordinator	**Marc Huger, marc.huger@unilim.fr, UNILIM**
Document Contributors	**Dietmar Gruber, dietmar.gruber@unileoben.ac.at, MUL** **Soheil Samadi, soheil.samadi@unileoben.ac.at, MUL** **Rafael Oliveira, rafael.oliveira@uc.pt, UMINHO** **Sina Darban, darban@agh.adu.pl, AGH** **Ilona Kieliba, kieliba@ghi.rwth-aachen.de, RWTH Aachen University** **Diana Vitiello, diana.vitiello@unilim.fr, UNILIM** **Robert Kaczmarek, robert.kaczmarek@unilim.fr, UNILIM** **Lucas Teixeira, lucas.breder-teixeira@univ-orleans.fr, UORL**

History of Changes

Version	Date	Author (Organization)	Change	Page
1.0	03.09.2020	Soheil Samadi (MUL)	Proposal – v1	All
2.0	22.09.2020	Rafael Oliveira (UMINHO)	Contribution	10
2.0	29.09.2020	Sina Darban (AGH)	Contribution	4
3.0	11.10.2020	Ilona Kieliba (RWTH) Diana Vitiello (UNILIM)	Contribution	3-5
4.0	20.10.2020	Robert Kaczmarek	Contribution	8
4.0	20.10.2020	Lucas Teixeira	Contribution	7-8
5.0	21.10.2020	Soheil Samadi	Contribution, Combining and Editing	All
5.1	26.10.2020	Dietmar Gruber	Proof reading	All
5.2	28.10.2020	Glyn Derrick	English check and formatting	All

European Commission | Horizon 2020 European Union funding for Research & Innovation

TABLE OF CONTENTS

1 Introduction

Due to the high temperature application of refractories, in-situ measurement and observation of their thermomechanical behaviour during application is difficult. In this regard, thermomechanical simulation of refractory lining behaviour is of great help. Determination of material mechanical properties is a prerequisite for modelling the behaviour of these materials as the properties are needed in FE-simulation. Several experimental approaches are thus defined here to identify different parameters for material models.

Different material models have been applied for mechanical behaviour simulation of refractory materials, which were explained in detail in deliverable 3.2 [1]. In service refractories experience thermal gradients and repetitive thermal shocks, which may generate significant stresses resulting in tensile failure of the material. On the other hand, due to thermal expansion, high compressive stresses are common in refractory materials, which may cause crushing of the material. The concrete damaged plasticity model, of the commercial software Abaqus [2], contains the tensile cracking model formulation as well as the compressive crushing model. The constitutive model uses the concept of isotropic damage evolution to represent the inelastic behaviour of the material. Additionally, to represent the shear failure, the Drucker-Prager model [3] is commonly applied. This model is mostly applied for materials in which the cohesion depends on the hydrostatic pressure. Finally, creep at high temperatures is very important in refractory linings because of its influence on the stress magnitude in the lining and in the steel shell. The classical Norton-Bailey creep model and Ducker-Prager creep model are available in Abaqus [2] for modelling of the creep behaviour of refractories [4].

This report will review the results obtained for the mechanical properties of the studied materials. This includes elastic material properties like Young's modulus and Poisson's ratio, thermomechanical properties like thermal expansion, fracture mechanical data, for example the tensile strength and the specific fracture energy, creep parameters and shear failure parameters such as cohesion and friction angle. The parameters were obtained either by direct measurement or by inverse evaluation of experimental results. The measurement devices were explained thoroughly in deliverable 1.3 and 1.4 [5,6]. Therefore, in this deliverable, only a short remark will be made regarding the experimental approach. Moreover, the focus of high temperature mechanical tests is on the shaped alumina spinel refractory material in the form of fired bricks, which are used in the working lining of the steel ladle. The application area of alumina spinel bricks in the steel ladle is shown in Figure 1.

European Commission | Horizon 2020 European Union funding for Research & Innovation

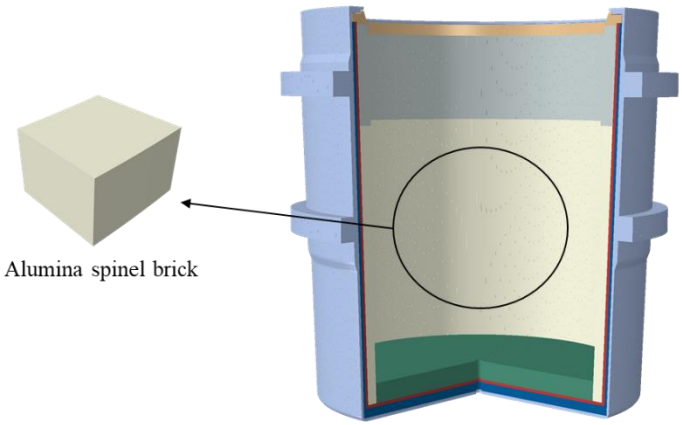

Figure 1: Area of application of alumina spinel bricks in the steel ladle

2 Elastic behaviour properties

Young's modulus and Poisson's ratio are the basic parameters necessary for thermomechanical simulation of refractory linings with all kinds of material constitutive models. Poisson's ratio does not vary as much as Young's modulus for refractories; the average value for refractories is 0.15 according to the refractories' handbook [7], and it can be defined the same in thermomechanical simulations. Hence, no Poisson's ratio measurements have been made in this deliverable. Furthermore, the thermal expansion shows the tendency of a material to change its volume or its dimensions due to a change in temperature. The thermal expansion coefficient is highly required since it is the main cause of mechanical strains and stresses in refractory linings.

2.1 YOUNG'S MODULUS

Two different non-destructive methods were used at room temperature, the ultrasonic method and the IET[1]; the IET was also employed at elevated temperatures. For the ultrasonic measurement, Young's modulus is calculated by measurement of sound velocity in the specimen; one pulse of ultrasonic energy is sent from a transducer into the specimen and received on the opposite side of the specimen [8]. The IET (RFDA[2] test) measures the resonance frequencies, and their damping, for rectangular shaped samples. The results from the IET (RFDA test) depend on the elastic properties (Young's and shear moduli), the geometry and density of the sample and the excitation method [9]. Firstly, the Young's modulus of the sample was measured with both methods at room temperature. Then the sample was heated up to 1500 °C (with a rate of 5 °C /min) and cooled, at the same rate, to room temperature in the furnace. The real-time measurements were recorded every minute with the final measurement recorded at room temperature using both methods. Three samples were considered for this case. The results of room temperature assessments of the Young's modulus can be found in Table 1. An increase in Young's modulus is detected with both techniques after heating, with the ultrasonic method results being slightly higher (about 4 GPa) than those of IET.

Table 1 : Results of Young's modulus measurement at room temperature before and after heating the samples

	Sample 1		Sample 2		Sample 3	
	Before Heating	After Heating	Before Heating	After Heating	Before Heating	After Heating
Ultrasonic method	35.32	39.04	42.66	46.66	38.17	41.07
IET	30.24	32.88	40.94	42.47	34.28	37.80

The evolution of Young's modulus during heating and cooling is shown in Figure 2. At first, the Young's modulus value decreased slightly and then increased on heating. During the cooling phase, the Young's modulus increased further reaching its highest value, before decreasing with further cooling. An average value of the three curves in Figure 2 will be used for the thermomechanical simulation.

[1] Impulse Excitation Technique

[2] Resonance Frequency Damping Analysis

European Commission | Horizon 2020 European Union funding for Research & Innovation

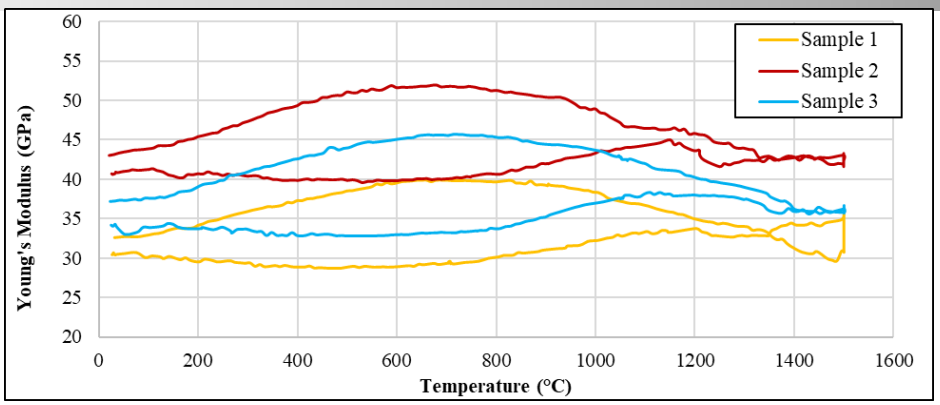

Figure 2: Young's modulus evolution diagram (RFDA high temperature results)

2.2 THERMAL EXPANSION COEFFICIENT

Dilatometry measurements yield precise information on dimensional changes, such as expansion or shrinkage, during a heating/cooling cycle. The measurement is based on a pushrod technique, which means that dimensional changes are detected by the displacement system with a pushrod, connected to the sample undergoing microstructural changes. The equipment measures the change in length as a function of temperature, and the linear coefficient of thermal expansion (CTE) is then calculated with Equ. 1:

$$\mathrm{CTE} = \frac{1}{L_0}\frac{\Delta L}{\Delta T} \qquad \text{Equ. 1}$$

Where L_0 is the initial length of the sample. Thermal expansion values maybe influenced by multiple factors such as material anisotropy, thermal history e.g. the firing temperature and duration, repeated firing and measurement conditions like atmosphere, pressure and heating rate. Figure 3 illustrates the influence of heating rate on thermal expansion coefficient on alumina spinel brick under investigation.

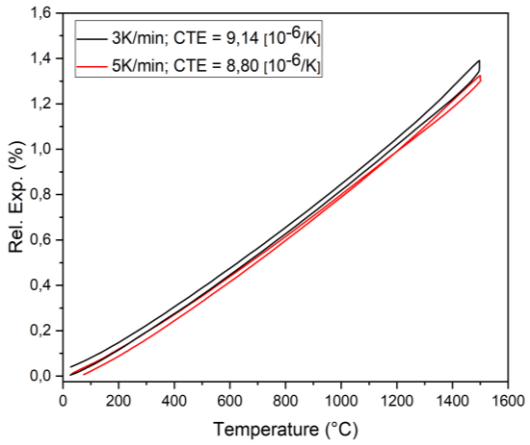

Figure 3: Relative expansion versus temperature with calculated CTE (30 - 1500 °C) determined at different heating rates for alumina spinel brick

Thermal expansion can also be measured alternatively by the apparatus used for Refractoriness Under Load / Creep in Compression (RUL/CIC). This measurement technique in fact allows for the measurement of bigger samples (cylindrical test piece: 50 mm in diameter and height with coaxial bore of 12.5 mm) comparing to standard dilatometry test pieces (rectangular shape: 5 x 5 x 25 mm^3), which may be advantageous for materials containing bigger aggregates like refractories. One important phenomenon that can be investigated using this testing approach is the effect of thermal shock on the thermal expansion characteristics.

In this regard, the basic hypothesis is that the material damage caused by the thermal shock triggers sintering phenomena and it gets more significant with the increase of damage and stress level. Once sintering starts, surface energy is consumed through particle bonding, resulting in increased strength and often a dimensional change. Therefore, thermal hysteresis curves can be used to monitor and estimate the degree of re-sintering and crack-healing phenomena. With the progress of material damage, the length and density of cracks increase and a complex state of stress with local stress concentrations develops, resulting in increased system energy. At this stage, the natural tendency of the system is to reduce the energy; therefore, at high temperatures, various mass transport mechanisms are activated to move particles from convex to concave surfaces and particles

European Commission | Horizon 2020 European Union funding for Research & Innovation

from compressive to tensional stress fields. Figure 4 shows the influence of thermal shock on thermal expansion characteristics of the alumina spinel brick obtained using RUL/CIC apparatus. In the conducted experiment, material shrinkage was observed after the second thermal shock, which indicates that damage induced by two thermal shocks triggered re-sintering and crack-healing phenomena. This phenomenon was not observed after the first thermal shock, which could indicate that level of material damage at this stage was not sufficient to induce mass transport phenomena.

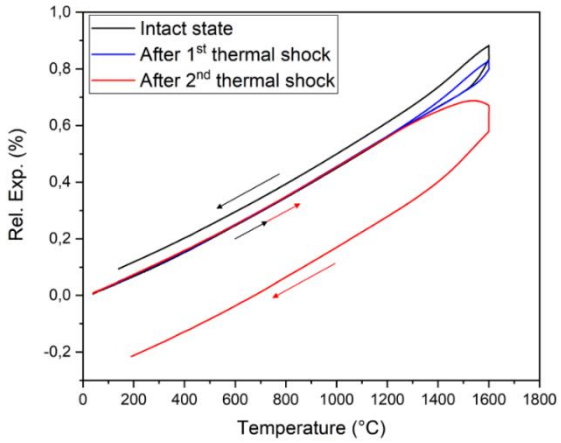

Figure 4: Influence of thermal shock on relative thermal expansion in case of alumina spinel brick

The CTE can be obtained from these curves and input into the simulation; normally it is defined to evolve only to heating and only the first cycle is considered. The thermal shock effect on the CTE might be considered by writing additional subroutines to be used in Abaqus. Microcracking also affects the CTE value and can be defined using other material constitutive models such as damage models.

3 Creep behaviour properties

In order to consider creep in thermomechanical simulations, creep law parameters are required as input data in the model. In this regard, two advanced experimental set-ups were developed for characterization of compressive and tensile creep behaviour of ceramic refractory materials [10,11]. Many models have been suggested to describe the creep behaviour of materials in terms of stress, time and temperature, among which the Norton-Bailey creep law is mostly applied. After obtaining strain/time data from both compressive and tensile creep tests, these data are employed with an inverse estimation method in order to determine the creep law parameters. The experiments were completed at three different temperatures and three different forces, in total 9 loading conditions (three specimens at each force and temperature).

The test plan for compressive creep is shown in Table 2:

Table 2: Compressive creep Loading conditions

Temperature (°C)	1300	1400	1500
Applied stress (MPa)	8 – 9 – 10	4 – 4.5 – 5	3.5 – 4 – 4.5

The test plan for tensile creep was as below:

Table 3: Tensile creep Loading conditions

Temperature (°C)	1200	1300	1400
Applied stress (MPa)	0.25 – 0.35 – 0.45	0.15 – 0.2 – 0.25	0.12 – 0.15 – 0.18

Concluding these test plans required several trial experiments to reach loads and temperatures with which all three stages of creep could be observed in a reasonable amount of time. The results of uniaxial compressive tests were plotted in Figure 5. The uniaxial compressive creep tests were done at 1300 °C, 1400 °C and 1500 °C.

European Commission | Horizon 2020 European Union funding for Research & Innovation

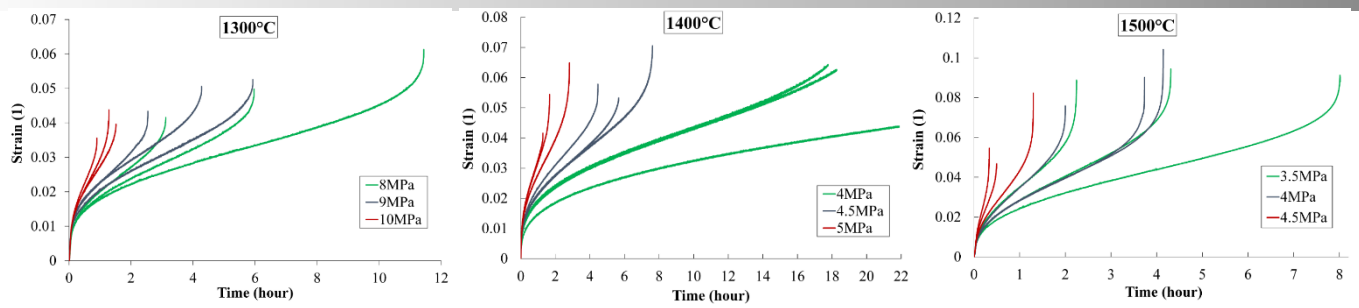

Figure 5: Compressive creep test results of the alumina spinel brick [12]

The results of uniaxial tensile tests were plotted in Figure 6. The uniaxial tensile creep tests were done at 1200 °C, 1300 °C and 1400 °C.

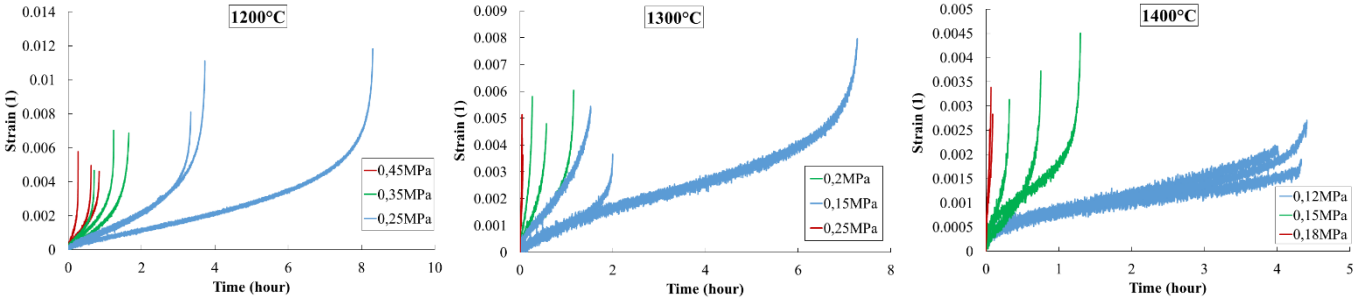

Figure 6: Tensile creep test results of the alumina spinel brick [14]

A short primary stage and a significant secondary creep stage were received in uniaxial tensile creep tests in contrast to the uniaxial compressive creep tests, in which both stages were significant. A high asymmetry existed in the creep behaviour of the alumina spinel brick. As it is shown in Figure 5 and Figure 6, tensile failure creep strain was much lower than the compressive failure creep strain.

After obtaining the results, an inverse evaluation method is applied to evaluate Norton-Bailey creep parameters "*a-n-K*" [10]. Input data for the inverse evaluation method can be selected in different ways; principally, a minimum of two curves with different constant stresses are necessary. This makes many possible ways of choosing the input data. In case of a completely homogeneous material, this different input data would result in the same creep parameters, but when there is scatter in the experimental results, different input data might generate different creep parameters. Therefore, a statistical study approach was conducted to investigate the heterogeneity of the material and its effect on the creep parameters [12]. In this approach, all the possible combinations from $\binom{9}{2}$ (2 out of 9 curves) to $\binom{9}{9}$ were chosen as the input datasets (8 in total), in a way that at least two different stresses exist. To explain more, in the dataset "Combination of 2", the minimization algorithm, tries to find the creep parameters of the best fitting curves to only two curves, and int the dataset "Combination of 9", it tries to find them for nine curves. Datasets populations are shown in Table 4.

Table 4 : Dataset population

Dataset	Combination of 2	Combination of 3	Combination of 4	Combination of 5	Combination of 6	Combination of 7	Combination of 8	Combination of 9
Dataset population	27	81	126	126	84	36	9	1

To compare the different dataset results, the mean value and standard deviation were calculated; additionally, to assess the representative of mean values from various combinations, confidence intervals for creep parameters in different datasets were obtained using the following equation.

$$|\mu - \bar{y}| \leq \frac{t_{\frac{\alpha}{2},n-1} S}{\sqrt{n}} \rightarrow \begin{cases} \mu: \text{population mean value} \\ \text{n}: \text{ dataset population} \\ \text{n}-1: \text{ degrees of freedom} \\ \alpha: \text{significance level of the test} \end{cases} \qquad \text{Equ. 2}$$

The right side of Equ. 2 is called "100(1- α) percent confidence interval" for the mean difference. *t* is obtained from the t-distribution table based on the degree-of-freedom of dataset and chosen confidence interval percentage "100(1- α)" [13]. A confidence interval percentage of 99% was chosen in this study.

European Commission | Horizon 2020 European Union funding for Research & Innovation

Based on this investigation, the dataset that is the better representative of the material scatter could be chosen. For instance, in the case of the primary creep stage of the compressive creep curves, the dataset "Combination of 7" was recommended [12]. For more detailed discussion on the topic, please refer to the references [12,14]. Here, the uniaxial compressive and tensile creep parameters were reported for primary creep stage in Table 5. It was observed that the standard deviation of creep parameters was higher in case of tensile creep results compared to the compressive creep curves. The parameters are representative for the scatter of the experimental results.

Table 5: Uniaxial compressive and tensile creep parameters for the primary creep stage

Primary creep stage	Representative parameters			
	Temperature (°C)	**n**	**a**	**Log(K[MPa^{-n}s^{-1}])**
Compressive creep parameters	1300	4.24 ± 0.22	-2.72 ± 0.07	-14.37 ± 0.25
	1400	5.88 ± 0.68	-2.65 ± 0.24	-13.75 ± 0.70
	1500	2.02 ± 0.55	-1.93 ± 0.10	-9.73 ± 0.44
Tensile creep parameters	1200	2.94 ± 0.82	-1.01 ± 0.40	-8.40 ± 1.31
	1300	5.72 ± 1.45	-1.75 ± 0.34	-7.56 ± 2.10
	1400	7.65 ± 1.42	-1.90 ± 0.36	-5.87 ± 1.97

For tensile creep behaviour, one approach might be to ignore the primary creep stage due to its relatively short duration [15]. In this regard, the secondary creep stage parameters obtained from samples tested at 1300 °C under tensile creep are shown in Table 6. Two approaches are considered: in the first one, all nine curves are considered. In the second case, only the two curves with more similar results are considered, under the assumption that outliers can appear due to imperfections in the tests procedures. It is clear that with reduced number of curves the standard deviation of the parameters is reduced.

Table 6: Uniaxial tensile creep parameters for the secondary creep stage at 1300 °C

	n	**Log(K[MPa^{-n}s^{-1}])**
All curves	11.68 ± 1.75	2.26 ± 1.12
Reduced number of curves	11.45 ± 0.19	2.19 ± 0.12

Moreover, another approach to consider both primary and secondary creep together for compressive creep modelling is to use a transient creep model. According to Naumenko and Altenbach [16], transient creep behaviour can be modelled considering a kinematic hardening visco-plastic law, having the back-stress as an additional state variable, according to Equ. 3.

$$\begin{cases} \dot{\bar{\varepsilon}}_{cr} = \frac{3}{2}\frac{\bar{s}}{\bar{\sigma}_{eq}} a \bar{\sigma}_{eq}{}^{n} \\ \dot{\bar{\beta}} = \frac{2}{3} b \dot{\bar{\varepsilon}}_{cr} - c \alpha_{eq}{}^{n-1} \bar{\beta} \\ \alpha_{eq} = \sqrt{\frac{3}{2}\bar{\beta} : \bar{\beta}} \end{cases} \qquad \text{Equ. 3}$$

The inverse evaluated parameters using this approach are shown in Table 7.

Table 7: Transient compressive creep parameters at 1300 °C

n	**Log(a[MPa^{-n}s^{-1}])**	**Log(b[MPa(1+scMPa^{n-1}])**	**Log(c[MPa^{-n}(MPa+b)/s])**
1.98 ± 0.69	-6.31 ± 0.64	2.56 ± 0.09	-5.01 ± 0.68

Figure 7 shows an example of the primary and secondary creep curves obtained at 1300 °C, as well as the curves resulting from the identification procedure using the transient creep law. It can be observed that the identification provides an accurate fit of the

European Commission | Horizon 2020 European Union funding for Research & Innovation

experimental curves. The curves identified using the primary creep law are also shown, to allow a comparison between the two assumptions.

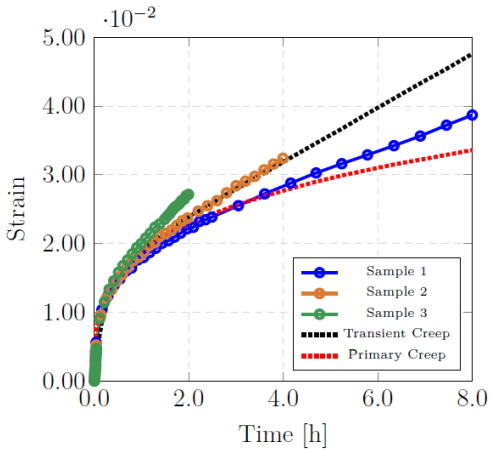

Figure 7: Transient creep identification at 1300 °C

4 Tensile failure properties

Tensile failure occurs for refractory materials in application due to different reasons such as thermal shock. Cracking in the lining and further spalling of the material are the consequences of tensile failure. In FEM simulation, concrete damaged plasticity has been widely used to reproduce tensile cracking behaviour. This model was explained in deliverable report 3.2 [1]. An experimental approach is necessary to obtain the model parameters for the desired material. Several testing methods have been proposed for the study of cracking behaviour of materials such as uniaxial tensile test, three-point bending test, wedge splitting test, etc.

The uniaxial tensile test has been introduced in the deliverable report 1.4 [6]. Using this test, alumina spinel bricks were tested at ambient temperature, with cyclic increase of load (Figure 8). Tests performed at ambient temperature determined values for; Young's modulus (E=11.6 GPa), tensile strength (f_t=1.57 MPa) and strain at maximum load (ε_t=0.024 %).

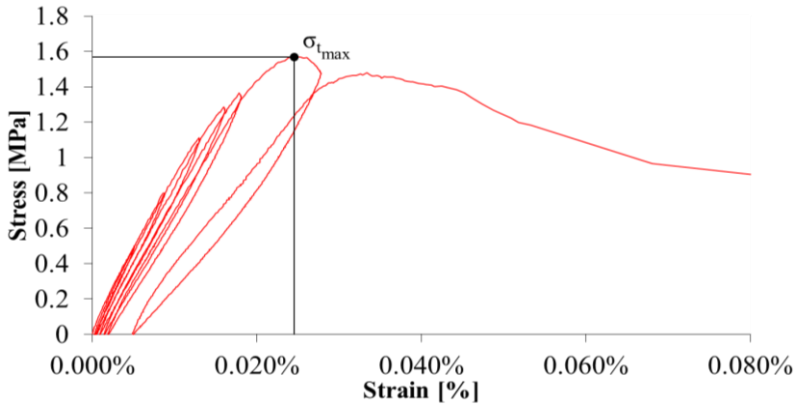

Figure 8: Stress-strain curve from a direct tensile test performed on alumina spinel brick at ambient temperature.

The wedge splitting test enables stable crack propagation even for relatively large specimen dimensions. It is used to characterize the mode 1 fracture phenomenon [17,18]. Results are received in form of load displacement diagrams, from which the following parameters can be directly calculated: specific fracture energy (G_f') and nominal notch tensile strength (σ_{NT}). The specific fracture energy is the area below the load-displacement curve divided by the fracture surface area. This parameter includes only the major part of the fracture energy because a premature termination of the test is necessary to avoid the contact of the wedge with the ligament. The nominal notch tensile strength is calculated using Equ. 4.

$$\sigma_{NT} = \frac{F_{H,max}}{\mathrm{bh}}\left(1 + \frac{6y}{h}\right) \qquad \text{Equ. 4}$$

where $F_{H,max}$ denotes the maximum horizontal force, b and h are the width and the height of the ligament, and y is the vertical distance from the loading position to the centre of the ligament. The experiment was done at three different temperatures (three specimens per temperature): room temperature, 1200 °C and 1400 °C. The new apparatus, developed in Ref. [19], allows for high-temperature WST tests with direct displacement measurements on the sample using a laser speckle system. The results of

European Commission | Horizon 2020 European Union funding for Research & Innovation

the wedge splitting tests were plotted in Figure 9. It was observed that the maximum applied load decreased with increasing temperature and the material became less brittle.

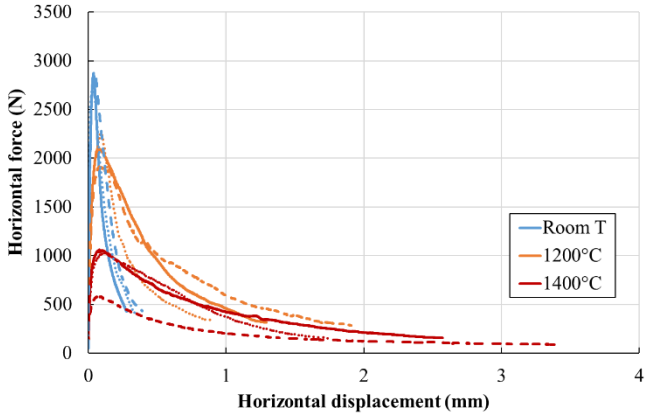

Figure 9: Load-displacement curves from wedge splitting tests at different temperatures

The specific fracture energy (G_f') and nominal notch tensile strength (σ_{NT}) were obtained using the curves and are shown in Figure 10. The nominal notch tensile strength decreased at higher temperatures. However, the mean value of the specific fracture energy increased from 112N/m at room temperature to 292N/m at 1200 °C and then decreased to 221N/m at 1400 °C.

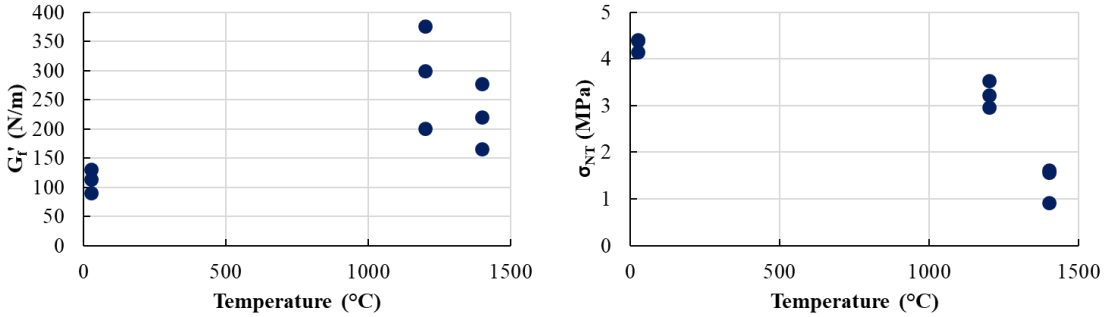

Figure 10: Specific fracture energy (G_f') and nominal notch tensile strength (σ_{NT}) at different temperatures

Although these parameters can be used for comparison of different refractories, they cannot directly be used in the simulation since they are estimated values using experimental results and not the exact material parameters. The fracture energy and tensile strength are the necessary values for material models and are inversely evaluated with the aid of modelling. In the literature, different modelling approaches have been used to simulate the wedge splitting test, and inversely evaluate the material parameters. In the study of Jin et al., cohesive elements with fictitious crack model, considering different softening behaviour laws, were assigned to the ligament and elastic behaviour was considered in the bulk of the material. The study proved that using bilinear and trilinear post-peak behaviour for the softening law generates better fittings to the experimental curves [20]. The concrete damaged plasticity (CDP) model implemented in Abaqus is also used to model fracture behaviour of quasi brittle materials [2]. In Table 8, the parameters necessary to be used in the CDP model, according to Figure 11, are shown for the three temperatures of experiments.

European Commission | Horizon 2020 European Union funding for Research & Innovation

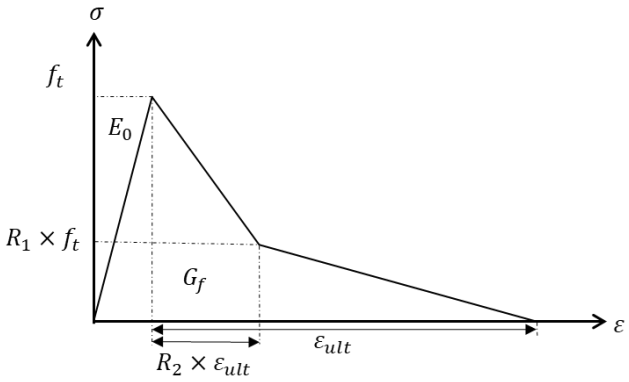

Figure 11: Bilinear fracture model

Table 8: Inverse evaluated fracture parameters using wedge splitting test

Parameter	Room temperature	1200 °C	1400 °C
G_f (Nm/m²) (mean ± STD)	136.0 ± 21.9	337.5 ± 90.8	258.7 ± 67.1
f_t (MPa) (mean ± STD)	2.91 ± 0.33	1.66 ± 0.16	0.68 ± 0.21
R_1	0.213	0.239	0.272
R_2	0.295	0.263	0.305

5 Compressive failure properties

The material's behaviour in compression may be obtained from compressive strain-stress curves. The compressive tests determine the compressive strength (f_c) at both room and elevated temperatures. The tests were performed on samples extracted from two types of alumina spinel bricks and in two directions (parallel or perpendicular to the pressing direction). Four series of tests were performed: Series 1: ø50 x 120 mm samples extracted from edged bricks, in the direction of pressing, tested at room temperature; Series 2: ø50 x 100 mm samples extracted from rectangular bricks, in the direction of pressing, tested at room temperature; Series 3: ø50 x 50 mm samples extracted from rectangular bricks, in the direction perpendicular to the direction of pressing, tested at room temperature; Series 4: ø50 x 100 mm samples extracted from the rectangular brick, in the direction of pressing, tested at elevated temperatures. The samples were placed in the testing machine and compressed under strain control at the rate of 0.01 % s^{-1} to have the same strain for different sample heights. Series 4 was tested at elevated temperatures (600 ºC, 800 ºC and 1000 ºC) with a heating rate of 5 ºC per minute. The overall results can be seen in Table 9. As expected, the resistance of the brick was higher in the pressing direction. The standard deviation of test results was up to 15 %; this was expected, as the setting method and positions of the bricks in the kiln during firing affect its mechanical properties [12,21].

Table 9: compressive strength of alumina spinel bricks

Series	Direction	Temperature	f_c [MPa] (mean ± STD)
S01	Pressing	20ºC	29.20 ± 3.20
S02	Pressing	20ºC	32.43 ± 3.65
S03	Perpendicular to Pressing	20ºC	27.43 ± 0.16
S04	Pressing	600ºC	24.21 ± 2.38
S04	Pressing	800ºC	34.35 ± 1.69
S04	Pressing	1000ºC	27.00 ± 4.08

6 Shear failure properties

The Drucker-Prager model [3], available in the software Abaqus [2], can be used to simulate granular materials and reproduce pressure-dependent yielding behaviour, i.e., the material becomes stronger as the pressure increases. This model is used to simulate materials in which the compressive yield strength is greater than the tensile yield strength [3]. The modified shear test is

European Commission | Horizon 2020 European Union funding for Research & Innovation

a testing method for the determination of the cohesion and the friction angle in Drucker-Prager failure criterion. Rectangular specimens (37.5 x 37.5 x 150 mm³) with notches of different angles (60° and 80°) are used in this test (Figure 12). The maximum force results, from the tests with different notch angles, were used to determine the cohesion and the friction angle from the p-q diagram, shown in Figure 12, connected with the Drucker-Prager failure criterion [22]. This experiment allows the determination of these parameters even at high temperatures. Three different temperatures (three specimens per temperature) were considered: room temperature, 1000 °C and 1200 °C. The results were plotted in Figure 13.

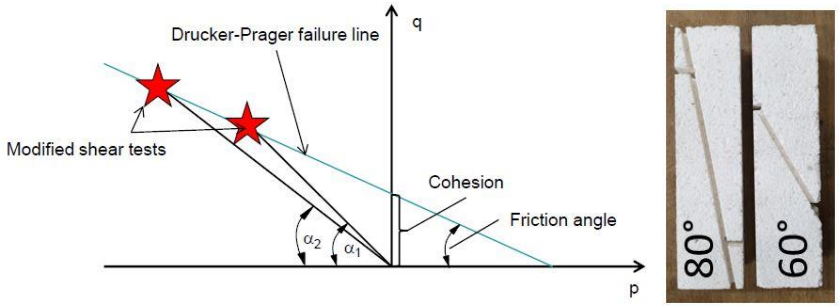

Figure 12: Drucker-Prager yield criterion (left), modified shear test specimens (right)

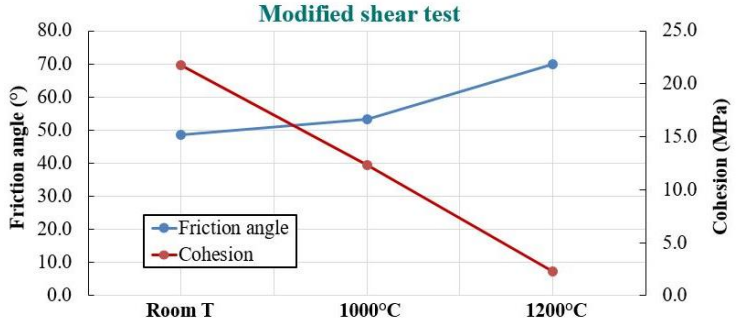

Figure 13: Drucker-Prager model parameters for alumina spinel brick at different temperatures

The friction angle is shown to increase, with increasing temperature, while the cohesion decreases. These results indicate that the material resistance to shear loads is much lower at high temperatures.

7 Conclusion

In this report, all the necessary material mechanical parameters for FEM simulation were reported for the alumina spinel refractory brick, which is the working lining material in the steel ladle. Due to its role, the alumina spinel bricks receive the most complicated and highest thermal, mechanical, and chemical loads. The data reported here included a complete view on the mechanical behaviour, from elastic material properties to fracture, mechanical and creep data. The usage of these parameters in FEM simulation of refractory linings will be described in following deliverables.

8 References

[1] S. Samadi, L. Teixeira, G. Derrick, and D. Gruber, “Deliverable D3.2: benchmark of the different thermomechanical behaviour models in commercial software applied to refractories”, 2020.
[2] ABAQUS (2018) ‘ABAQUS Documentation’, Dassault systems, Providence, RI, USA.
[3] D.C. Drucker, W. Prager, “Soil mechanics and plastic analysis for limit design”, Quarterly of Applied Mathematics, 1952, 10, 2, 157–165.
[4] S. Jin, H. Harmuth, D. Gruber, R. Rössler, “Creep modelling of Magnesia-chromite bricks in a RH snorkel during a process cycle”, China’s Refractories, 2015, 24, 22-25.
[5] D. Vitiello, I. Kieliba, G. Derrick, and M. Huger, “Deliverable D1.3: devices for thermo-physical properties characterisation”, 2019.
[6] H.T. Nguyen, S. Samadi, L. Teixeira, F. Asadi, R. Kaczmarek, I. Kielibla, V. Tadaion, T. Tonnesen, E. Blond, M. Huger, D. Gruber, “Deliverable D1.4: devices for mechanical characterisation at laboratory scale that are operational”, 2019.
[7] Ch. Schacht, ed. Refractories handbook. Vol. 178. CRC Press, 2004.
[8] J.P.L. Dos Santos, P.M. Amaral, A.C. Diogo, L.G. Rosa, “Comparison of Young’s moduli of engineered stones using different test methods”, Key engineering materials, 2013, 548, 220-230.

European Commission | Horizon 2020 European Union funding for Research & Innovation

[9] W. Weglewski, K. Bochenek, M. Basista, Th. Schubert, U. Jehring, J. Litniewski, S. Mackiewicz, "Comparative assessment of Young's modulus measurements of metal–ceramic composites using mechanical and non-destructive tests and micro-CT based computational modelling" Computational materials science, 2013, 77, 19-30.
[10] S. Jin, H. Harmuth, D. Gruber, "Compressive creep testing of refractories at elevated loads—Device, material law and evaluation techniques", Journal of the European ceramic society, 2014, 34, 4037-4042.
[11] A. Sidi Mammar, D. Gruber, H. Harmuth, S. Jin, "Tensile creep measurements of ordinary ceramic refractories at service related loads including setup, creep law, testing and evaluation procedures", Ceramics international, 2016, 42, 6791-6799.
[12] S. Samadi, S. Jin, D. Gruber, H. Harmuth, S. Schachner, "Statistical study of compressive creep parameters of an alumina spinel refractory" Ceramic Internationals, 2020, 46(10–A), 14662–14668.
[13] C.D. Montgomery, "Design and analysis of experiments", 2017, Wiley.
[14] S. Samadi, L. Teixeira, S. Jin, D. Gruber, H. Harmuth, "Creep parameter determination of a shaped alumina spinel refractory using statistical analysis", Proceedings of 63rd International Colloquium on Refractories, Raw Materials and Reuse, pp. 1–5. 2020.
[15] L. Teixeira, S. Samadi, J. Gillibert, S. Jin, T. Sayet, D. Gruber, E. Blond, "Experimental investigation of the tension and compression creep behavior of alumina-spinel refractories at high temperatures", Ceramics, 2020, 3, 372-383.
[16] K. Naumenko, H. Altenbach, "Modeling of creep for structural analysis", Red. By V. I. Babitsky and J.Wittenburg, Foundations of Engineering Mechanics, 2007, Berlin, Heidelberg: Springer Berlin Heidelberg.
[17] H. Harmuth, K. Rieder, M. Krobath, E. Tschegg, "Investigation of the nonlinear fracture behaviour of ordinary ceramic refractory materials", Materials Science and Engineering: A, 1996, 214, 53–61.
[18] E. Tschegg, "Equipment and appropriate specimen shapes for tests to measure fracture values", Austria Patent 390328, 31 January 1986.
[19] M. Stückelschweiger, D. Gruber, S. Jin, H. Harmuth, "Wedge-splitting test on carbon-containing refractories at high temperatures", Applied Sciences, 2019, 9(16), 3249.
[20] S. Jin, D. Gruber, H. Harmuth, "Determination of Young's modulus, fracture energy and tensile strength of refractories by inverse estimation of a wedge splitting procedure" Engineering Fracture Mechanics, 2014, 116, 228-236.
[21] R.A. Heindl, L.E. Mong, "Young's modulus of elasticity, strength, and extensibility of refractories in tension", Journal of Research of the National Bureau of Standards, 1936, 17, 463–482.
[22] E. Dahlem, "Characterization of refractory failure under combined hydrostatic and shear loading at elevated temperatures", Doctoral Thesis, Montanuniversität Leoben, 2011.

European Commission | Horizon 2020 European Union funding for Research & Innovation